Acid Hydrolysis to Provide the Potential for Rice-Husk-Derived C/SiO_2 Composites for Lithium-Ion Batteries

Lijie Ma[1] · Li Liu[2] · Xiaoyang Liu[1] · Yixin Li[1] · Yi Feng[1] · Yumei Tian[1] · Yimin Chao[3] · Yanchao Zhu[1] · Xiaofeng Wang

Abstract

As major waste materials in the rice milling industry, rice husks (RHs) have potential industrial applications. In this work, acid solutions were used to extract high-value-added polysaccharide components (hemicellulose and cellulose) from RHs to obtain sugar residues (SRs) for comprehensive utilization. The SRs were converted into C/SiO_2 composites after carbonization and ball-milling. The C/SiO_2 composites with crystalline cellulose content in the precursor possessed desirable electrochemical properties when tested as an anode material for lithium-ion batteries (LIBs), including cycle performance, initial Coulombic efficiency (ICE) and electrical impedance. Meanwhile, a high reversible specific capacity of 553 mAh g^{-1} was maintained after 100 cycles at a current density of 0.1 A g^{-1}. This method can be used to turn biomass into a potentially valuable anode material with desirable electrochemical properties for LIBs.

Keywords Rice husks · sugar residues · C/SiO_2 composites · lithium-ion battery

Introduction

Rice husks (RHs) are major waste products in the rice milling industry, and contain components of cellulose, hemicellulose, lignin, and silicate.[1,2] The traditional treatment of RHs, whether combustion or landfill, causes serious environmental pollution due to the high ash content of RHs.[3] As a consequence, the comprehensive utilization of the SiO_2 and C components of RHs have become a focus on scientific research,[4] and the natural composite structure of these two components makes it possible to apply RHs to the anode material for lithium-ion batteries (LIBs).[5,6]

In previous studies, RH-based C/SiO_2 composite materials were prepared by one-step carbonization of RHs, which were proven to have good electrochemical properties.[7,8] Wang et al. prepared C/SiO_2 material by calcining RHs directly, and the material exhibited a capacity of 485 mAh g^{-1} at a current density of 0.1 A g^{-1}, as well as superior cycling performance.[9] Cui et al. prepared micro-sized porous C/SiO_2 composites from RHs through a facile carbonization process under an Ar atmosphere with $ZnCl_2$ as an activating agent. The porous C/SiO_2 composite exhibited high discharge-specific capacity (ca. 1105 mAh g^{-1} at 0.1 A g^{-1}), stable cycling stability and good rate capability.[10] In these RH-based silica/carbon systems, SiO_2 possesses a high theoretical specific capacity of 1961 mAh g^{-1}, and could be a dominant contributor to the specific capacity of the anode material. Carbon provides conductivity for the anode material and maintains structural stability.[11] Therefore, the optimal utilization of RHs is to extract high-value-added polysaccharide components (hemicellulose and cellulose), which are applied to prepare xylose and ethanol in the sugar industry.[12,13] The retained sugar residues (SRs) contain lignin, silicate and unextracted cellulose, would be converted into the C/SiO_2 composite after a carbonization process and used as an anode material for LIBs.[14]

Hemicellulose, cellulose, and lignin have unique chemical properties due to their different structures and molecular

✉ Yanchao Zhu
yanchao_zhu@jlu.edu.cn

✉ Xiaofeng Wang
wangxf103@jlu.edu.cn

1 State Key Laboratory of Inorganic Synthesis and Preparative Chemistry, College of Chemistry, Jilin University, 2699 Qianjin Street, Changchun 130012, People's Republic of China

2 Department of Chemistry, Northeast Normal University, Changchun 130024, People's Republic of China

3 School of Chemistry, University of East Anglia, Norwich Research Park, Norwich NR4 7TJ, UK

weights. Hemicellulose is composed of heteropolymers with amorphous structures, which could be hydrolyzed by dilute acid to pentose (xylose, arabinose etc.).[15,16] Cellulose, as the main component of RHs, consists of chains of glucose linked by β-1,4 linkages.[12] The parallel cellulose chains form highly ordered and crystalline regions, which are interspersed by disordered and amorphous regions.[17] The amorphous regions are preferentially hydrolyzed by acid, whereas the crystalline regions are resistant to acid.[18] Lignin has a 3-D amorphous structure consisting of methoxylated phenylpropane, which is made up of *p*-coumaryl, coniferyl and sinapyl alcohols.[19] As a result of its complex structure, lignin is as resistant to acid dissolution as silicate.[20] Therefore, SRs could be obtained by acid extraction in the sugar industry, and C/SiO_2 composites containing different carbon components could be obtained after carbonization. In addition, ball-milling is employed to boost the combination of the C/SiO_2 composites, which results in the composites having excellent electrochemical properties for application as anode materials for LIBs.[21] However, the components of SRs are related to the extraction processes, and different content among these lignocellulosic components in SRs would lead to the formation of C/SiO_2 composites with substantially distinct features. Therefore, while extracting high-value-added polysaccharide components (hemicellulose and cellulose) from RHs, it is necessary to understand the influence of different lignocellulose components on the structural properties and corresponding electrochemical performance of C/SiO_2 composites derived from the SRs.

In this work, RHs were treated by acid solutions to hydrolyze hemicellulose and cellulose. The remaining SRs were carbonized, after which a ball-milling process was used to prepare C/SiO_2 composites. The suitability of the resulting composites for electrodes in LIBs was evaluated by using a series of electrochemical techniques. The composition of the SRs was manipulated by changing the conditions of acid hydrolysis so as to achieve comprehensive utilization of each component of the RHs. The conversion of SRs to battery materials is a highly energy-efficient process with great economic and environmental benefits.

Experimental

Preparation of Ball-Milled C/SiO_2 Composites

The raw RHs were bought from a rice mill around Changchun City, China. The RHs were washed with water, dried out in a 100°C oven and crushed into powders. Then, 100 g of the powdered RH was added into one of several 1000 mL solutions having different concentrations of hydrochloric acid or sulphuric acid. The concentrations of hydrochloric acid were 0.1 M, 1.0 M, and 3.0 M. The concentration of sulphuric acid was 12.0 M. The solutions were boiled with reflux for 2 h, followed by vacuum filtration. The filtrate residues were washed to neutral by distilled water and dried in the 100°C oven. The dried filtrate residues were calcined in a quartz tube furnace at 300°C for 0.5 h and then calcined at 700°C for 2 h under nitrogen with a heating rate of 5°C min^{-1}. After cooling to room temperature naturally, the C/SiO_2 mixtures were obtained and denoted as H0.1, H1.0, H3.0 and S, respectively, where H and S stand for HCl and H_2SO_4 treatment, respectively. In the ball-mill treatment, 3 g C/SiO_2 was loaded into a zirconia jar containing 90 g zirconia balls with non-uniform size. The ball-milling process was controlled at 800 rpm for 12 h and the C/SiO_2 composites were obtained and denoted as BM-H0.1, BM-H1.0, BM-H3.0 and BM-S respectively.

In addition, 100 g powders of RHs were carbonized and ball-milled in the same conditions as above. The obtained products were denoted as UT and BM-UT (UT meaning that the RHs were untreated with acid solution), respectively. The preparation process of the ball-milled C/SiO_2 composites is shown in Fig. 1.

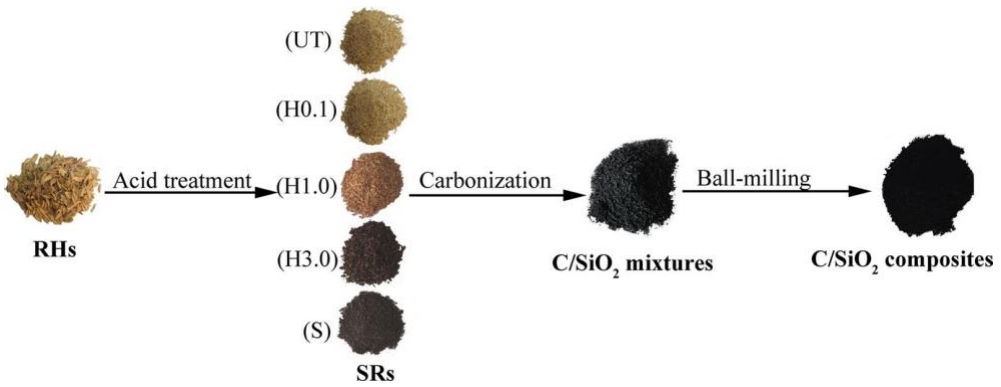

Fig. 1 The preparation process of C/SiO_2 composites.

Characterization

Thermogravimetric analysis (TGA) was carried out on a thermogravimetric analyzer (STA499F3, NETZSCH, Germany) from room temperature to 800°C at a heating rate of 20°C min^{-1} in air. The morphologies of the samples were observed by scanning electron microscopy (SEM, SU8020, HITACHI, Japan). The structure of the materials was characterized by an x-ray diffractometer using Cu Kα radiation (XRD, D/MAX2550, RIGAKU, Japan) operated at 50 kV and 200 mA with a scanning speed of 10°/min. Raman spectra were collected employing a Raman spectrometer (LabRAM HR Evolution, HORIBA, France) operating at an excitation wavelength of 473 nm.

Electrochemical Measurements

The working electrodes for the cells were fabricated by compressing a mixture of active material (80 wt. %), conductive material (acetylene black) (10 wt. %), and binder (polyvinylidene fluoride) (10 wt. %). Excess *N*-methyl-2-pyrrolidone (NMP) (a solid-liquid ratio of 1:50 m/v) was used, and the mixture was stirred over 5 h until a homogeneous slurry formed, which was coated on a copper foil. After drying at 80°C in a vacuum oven for 12 h, the composite anodes were punched into wafers with a diameter of 1.2 cm and an active material mass loading of 0.8-1.2 mg cm^{-2}. Coin-type half cells (2025R type) were assembled inside an Ar-filled glove box with lithium foils as counter electrodes and 1 M $LiPF_6$ in ethylene carbonate, ethyl methyl carbonate and diethyl carbonate (EC:EMC:DEC = 1:1:1, v/v/v) as electrolyte. Galvanostatic charge-discharge cycling was measured using a Neware CT-4008W battery test system from 0.01 to 3.0 V (versus Li/Li^+) at a current density of 100 mA g^{-1} and electrochemical impedance spectroscopy (EIS, in the range from 100 kHz to 0.01 Hz with an amplitude of 10 mV) was performed using a CHI 760D electrochemical workstation.

Results and Discussion

Using 100 g RHs as a base, the mass retention of the samples is shown in Table I. Due to the different susceptibility of the components to hydrolysis, the mass loss of the RHs is relative to the acid solutions. After treating with 0.1 M HCl solution, 68.9 g SR was retained, while the difference between the SRs after treating with 1.0 M and 3.0 M HCl solution was only 1.2 g (59.2 g and 58.0 g, respectively). Combined with the pictures shown in Fig. 1, the color of the H3.0 SRs was black, which was different from the brown color of the H1.0 SRs. This may be due to the dehydration of some organic components in the SRs by the 3.0 M HCl solution, resulting in a slightly higher mass loss than when using the 1.0 M HCl solution. When the HCl solution was replaced by 12.0 M H_2SO_4 solution, the mass loss was 68.4 g, which was more than the total content of hemicellulose and cellulose in the RHs (~ 54%)[22]. This occurred because the dehydration and strong oxidation characteristics of concentrated sulfuric acid led to large amounts of organic components being dehydrated.

Table I The mass retention of the samples and the results of TGA (based on the 100 g RHs)

The acid solution	The weighing results		The TGA results	
	The mass of SRs (g)	The mass of C/SiO_2 (g)	The mass of C (g)	the mass ratio of C to SiO_2
Untreated	100	37.2	21.6	1.4
0.1 M HCl	68.9	30.4	16.3	1.2
1.0 M HCl	59.2	27.5	13.1	0.9
3.0 M HCl	58.0	28.9	14.6	1.0
12.0 M H_2SO_4	31.6	22.4	7.7	0.5

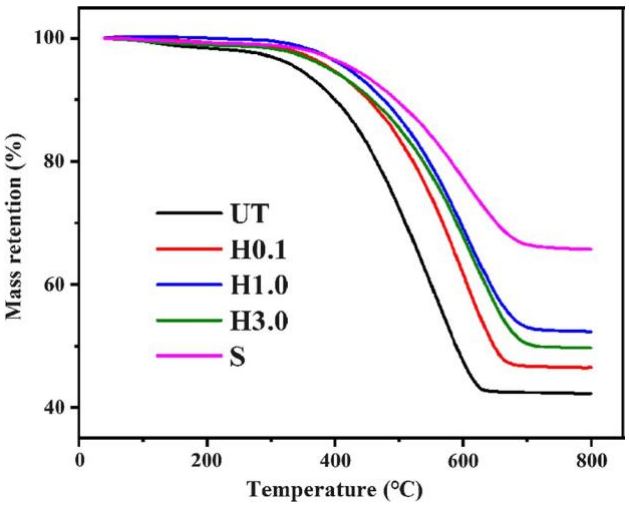

Fig. 2 TG curves of all C/SiO_2 mixtures.

Thermogravimetric (TG) curves under an air atmosphere are shown in Fig. 2 for the C/SiO_2 mixtures. The ratios of the mass losses of UT, H0.1, H1.0, H3.0, and S were 57.7%, 53.5%, 47.7%, 50.4% and 34.3%, respectively. As listed in Table I, the mass of carbon and the mass ratios of C to SiO_2 in C/SiO_2 mixtures were calculated. Based on the known contents of the main components in RHs (35.9% cellulose, 18.2% hemicellulose, 24.5% lignin, and 21.4% silicate),[22] the mass loss of the components in the RHs after acid treatment were calculated as follows and the results listed in Table II.

Table II The mass losses of components in RHs after acid treatment (based on 100 g RHs)

The acid solution	The mass loss after acid treatment (g)	
	Hemicellulose and cellulose	Inorganic salt and water
0.1 M HCl	23.9	7.2
1.0 M HCl	33.7	7.1
3.0 M HCl	34.8	7.2
12.0 M H_2SO_4	61.8	6.6

$$\begin{cases} x + y = 100 - m_{SRs} \\ \frac{m_C}{m_{SiO_2}} = \frac{C_c*(78.6-x)}{21.4-y} \\ C_c = \frac{m_C}{m_{precursors}} \end{cases} \quad (1)$$

where x is the total mass loss of hemicellulose and cellulose after acid treatment, y is the total mass loss of inorganic salt and water after acid treatment, and C_c is defined as char yield of the organic precursors. The total mass losses of hemicellulose and cellulose in RHs were higher than the theoretical content of hemicellulose (18.2%), and hemicellulose was more liable to be hydrolyzed by acid solution, indicating that the hemicellulose was completely hydrolyzed. After treating with 1.0 M HCl solution, about 15 g cellulose was hydrolyzed, accounting for 40% of total cellulose in RHs. According to the results reported by Ang et al.[14], it can be inferred that the amorphous part of the cellulose is hydrolyzed. The SRs (H1.0) contained crystalline cellulose, lignin and SiO_2. The total mass loss in 3.0 M HCl solution was a little higher, because the dehydration product was mixed into the SRs (H3.0). The impact of these carbons on performance will be discussed later.

The morphologies of the carbonized products of UT, H1.0 and S samples can be observed from SEM images shown in Fig. 3 a, b and c. The surface of the bulk carbon of the UT sample exhibited a smooth surface. The others were relatively rough due to corrosion by the acid solutions. Combined with the analysis of Tables I and II, the difference in surfaces surface could be related to the hydrolysis of cellulose and hemicellulose. This result would lead to differences in precursors and carbon contents of C/SiO_2 composites, and further affect the electrochemical properties of the resulting materials. Especially in the sample of S, the aggregated silica spheres were exposed on the surface of the bulk carbon (Fig. 3c), resulting in a lack of carbon to improve electronic conductivity and buffer volume changes during electrochemical lithiation/de-lithiation processes. After ball-milling, bulk carbon was broken and the particle sizes of the composites were significantly decreased. All samples had similar morphologies (Fig. 3d, e, f). Thus, it could be inferred that the ball milling is not the main reason for the difference of electrochemical properties.

The XRD patterns were shown in Fig. 4a. A broad peak observed between ~ 20° and ~ 26°, centered at ~ 23°, could be assumed to correspond to overlapping peaks of amorphous carbon and amorphous silica in the C/SiO_2 composites, another peak around 43°–44° was ascribed to the amorphous structure of carbon (C).[23] The peak at 23° of BM-H1.0 was sharper than that of the other samples,

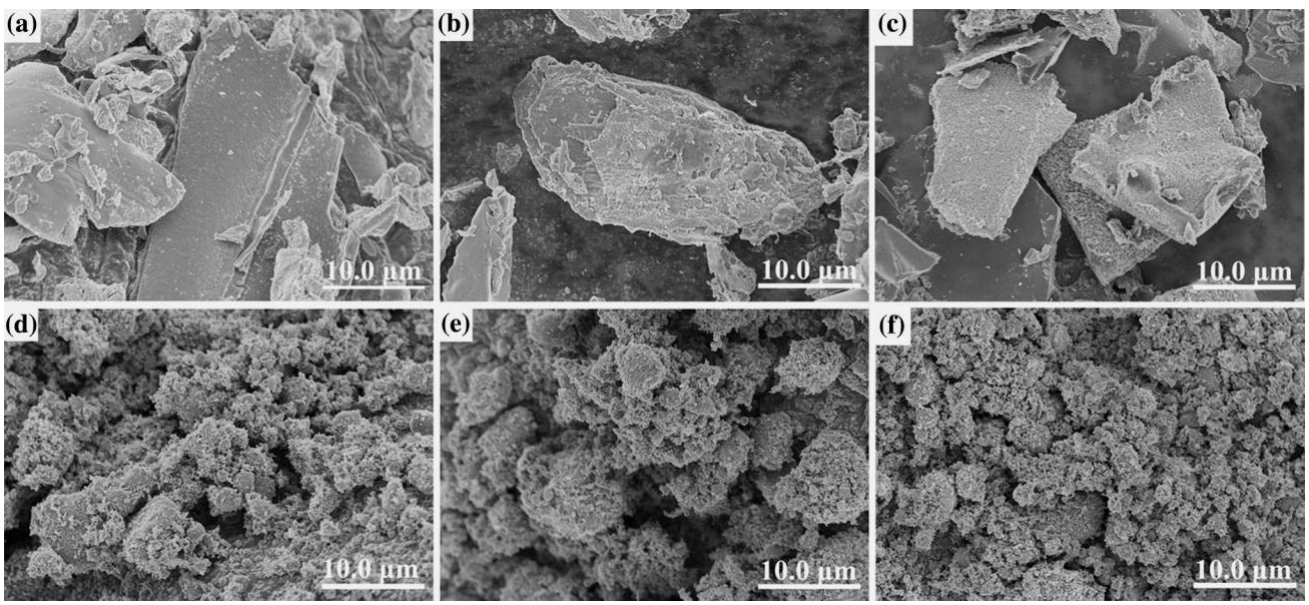

Fig. 3 SEM images of C/SiO_2 composites, (a) UT, (b) H1.0, (c) S (d) BM-UT, (e) BM-H1.0 and (f) BM-S.

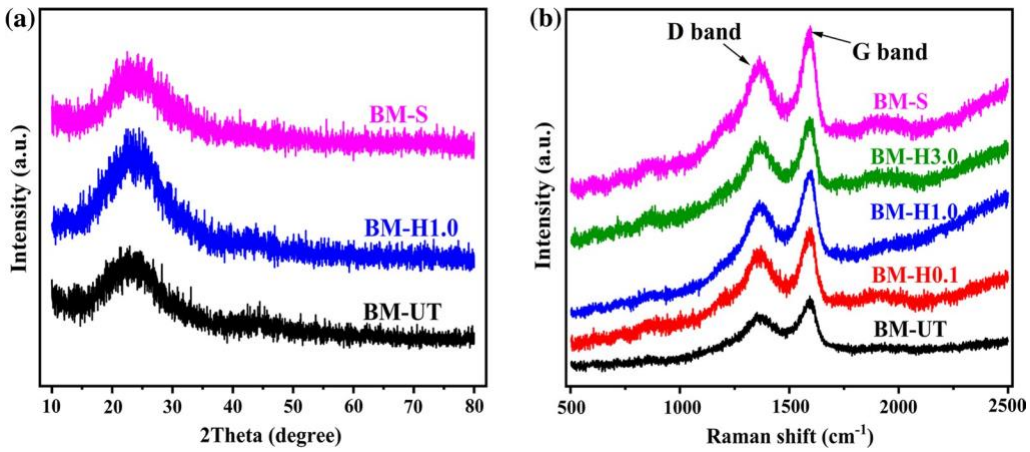

Fig. 4 (a) XRD patterns of BM-UT, BM-H1.0 and BM-S, (b) Raman spectra of all ball-milled C/SiO_2 composites.

because BM-H1.0 was rich in crystalline cellulose with no hemicellulose and amorphous cellulose, leading to more ordered carbons.

The Raman spectra of the C/SiO_2 composites is displayed in Fig. 4b. The peaks of the D-band and G-band at 1350 and 1590 cm^{-1} refer to disordered and sp^2-bonded carbon atoms, respectively. A lower value of I_D/I_G represents a higher degree of graphitized carbon in the composites.[21] The values of I_D/I_G for BM-UT, BM-H0.1, BM-H1.0, BM-H3.0 and BM-S were 0.87, 0.86, 0.84, 0.90 and 0.92, respectively. This illustrates that the degree of graphitized carbon varies depending on the precursor, which was consistent with the studies of Kim et al.[24]. The BM-UT resulted in a relatively high I_D/I_G value, while the BM-H0.1 (after removal of hemicellulose) showed a decreased I_D/I_G value. Due to the differences in the thermal stability of each monosaccharide unit in hemicellulose, the thermal degradation of hemicellulose takes place in a wide temperature range.[25] The carbon rearrangement could thus be hindered and lead to fewer sp^2 carbons, resulting in a higher degree of disorder for the carbon in BM-UT. BM-H1.0 had the lowest value of I_D/I_G, because the disordered components (hemicellulose and amorphous cellulose) were hydrolyzed by the 1.0 M HCl solution and the ordered components (such as crystalline cellulose) were preserved, which may promote the formation of sp^2 carbon and provide superior electrical conductivity within the carbon matrix. Further removal of cellulose then decreases the I_D/I_G value, because lignin is a highly thermo-resistant component due to its rich cross-linking. Due to the slow kinetics of thermal decomposition, the formation of an sp^2 structure could be substantially suppressed.[26]

Figure 5a shows the galvanostatic charge/discharge (GCD) profiles of BM-H1.0 at a current density of 0.1 A g^{-1}. The discharge-specific capacity (1st cycle and 100th cycle) and initial coulombic efficiency (ICE) of all C/SiO_2 composites are displayed in Table III. The first discharge- and charge-specific capacity of the BM-H1.0 composite were as high as 1185 and 664 mAh g^{-1} with an ICE of 56%, which was superior to the other composites because the high graphitized carbon content of the BM-H1.0 reduces irreversible Li^+ insertion capacity.[27] The curves at the 50th cycle and the 100th cycle nearly overlap, indicating that BM-H1.0 had excellent cycling stability. In addition, compared to the reported SiO_2-based composites (Table IV), the BM-H1.0 composites display similar or even better electrochemical performance, indicating the composites derived from RHs may be used as a promising anode material in LIBs. The simple acid hydrolyzing (without any expensive reagents or complex coating method) and ball-milling modification process described here is more economic and promising for preparation of C/SiO_2 composites. Figure 5b shows the capacity differential profiles at the first three cycles, which better illustrates the lithiation/delithiation processes. At the first cycle, the reduction peak at 1.3 V corresponded to the plateau in the GCD profiles, which could be attributed to the decomposition of the electrolyte and the formation of SEI film.[28] The peak disappeared in subsequent cycles and the curves tended to be stable, indicating that a stable SEI film had formed, which helps achieve desirable cycling performance.

Cycling performances of all C/SiO_2 composites at 0.1 A g^{-1} are shown in Fig. 5c. (All the materials were tested after the third cycle at 0.1 A g^{-1}, and the data for the first three cycles were not shown). The reversible capacity decayed slightly in the initial cycles and reached a relatively stable value in the rest of cycles. Among these five materials, BM-H1.0 had the highest discharge-specific capacity, as high as 553 mAh g^{-1} at 0.1 A g^{-1} after 100 cycles. This occurred because BM-H1.0 contained a large amount of silica that can provide specific capacity, and because this sample contained more graphitized carbon, which can promote the transport of lithium ions.[29] To further confirm

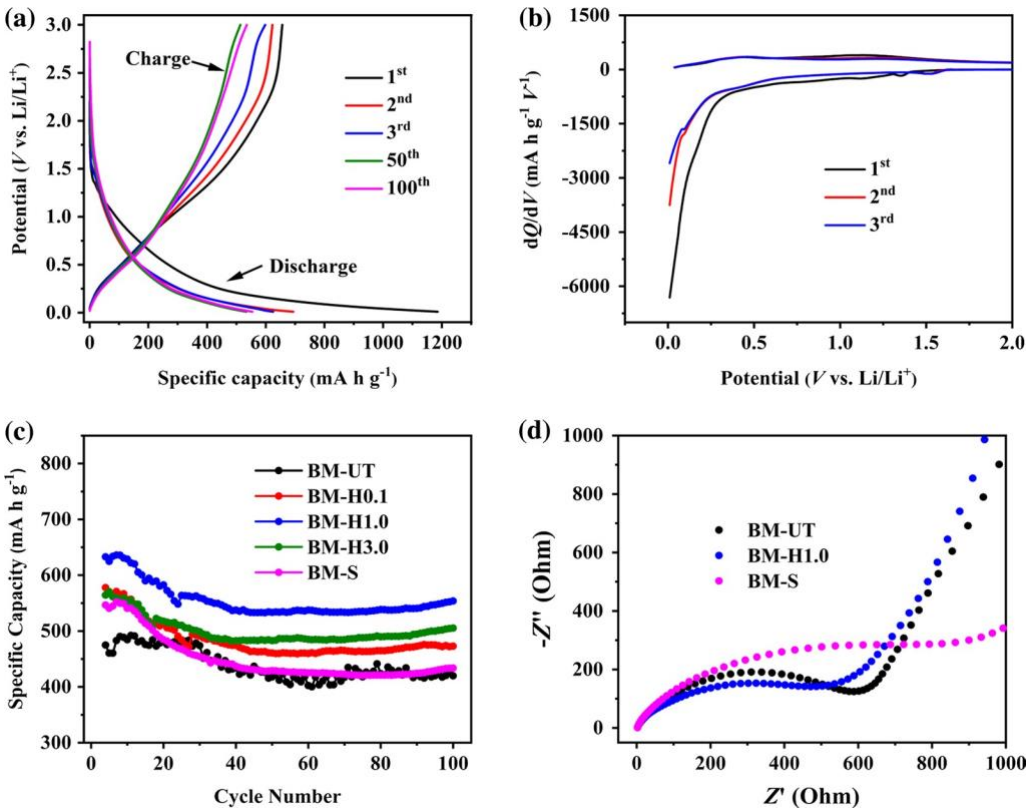

Fig. 5 (a) Galvanostatic charge-discharge (GCD) voltage profiles and (b) differential capacity plots (DCPs) at the first three cycles of BM-H1.0 at 0.1 A g^{-1}, (c) Cyclic performance at 0.1 A g^{-1} of all C/SiO_2 composites and (d) Nyquist plots before cycling of BM-UT, BM-H1.0, BM-S.

Table III The comparison results of cycling performances of ball-milled C/SiO_2 composites

Sample	Initial discharge-specific capacity (mAh g^{-1})	100th discharge-specific capacity (mAh g^{-1})	Initial Coulombic efficiency (%)
BM-UT	978	419	51
BM-H0.1	1163	472	54
BM-H1.0	1185	553	56
BM-H3.0	1110	505	52
BM-S	1106	433	50

the effect of the graphitized carbon on the electrochemical performance, the results of EIS tests are shown in Fig. 5d. Each Nyquist plot consists of a single semicircle in the high-frequency region and an inclined line in the low-frequency region, which represent charge transfer resistance (Rct) and lithium-ion diffusion resistance, respectively.[30] The diameter of the semicircle of BM-H1.0 was the smallest, because the high level of graphitized carbon could facilitate Li-ion insertion and extraction, and further lower resistance of the electrochemical reaction.

Table IV The comparison of specific capacities of the C/SiO_2 composites

Samples	Materials	Methods	Specific capacity	References
pp-MSNs/FG	Graphite oxide, colloidal silica, sucrose	Hydrothermal method	702 mAh g^{-1} (100th, 0.1 A g^{-1})	31
NFC-15 wt.%	PAN, SiO_2 nanoparticles	Electrospinning	658 mAh g^{-1} (100th, 50 mA g^{-1})	32
SiO_2/C/graphene	TEOS, PVP, graphene oxides	Suspension nebulization and spray pyrolysis method	610 mAh g^{-1} (100th, 50 mA g^{-1})	33
SiO_2 /C@SiO_2 @CNT	CNTs, TEOS, resorcinol, formaldehyde	Self-assembly	644 mAh g^{-1} (200th, 0.1 A g^{-1})	34
BM-H1.0	Rice husks (RHs)	Acid hydrolyzing	553 mAh g^{-1} (100th, 0.1 A g^{-1})	This work

Conclusions

In summary, SRs were extracted from RHs by an acid solution and C/SiO_2 composites were obtained by carbonization, followed by a ball-milling process to boost the combination of C and SiO_2. BM-H1.0 maintained a high, reversible specific capacity of 553 mAh g^{-1} at 0.1 A g^{-1} over 100 cycles. The SR (H1.0) has the highest content of crystalline cellulose, which leads to BM-H1.0 having the most graphitized carbon to promote the transport of lithium ions. This result indicates that the composition of the major components of the SRs were manipulated by changing the extraction processes of high-value-added polysaccharide components in RHs. The C/SiO_2 composites obtained by this method have desirable electrochemical properties. Thus, an economical and environment-friendly method was employed to comprehensively utilize RHs, providing a prospect for the application of biomass.

Acknowledgments We are grateful for financial support from the Graduate Innovation Fund of Jilin University (Nos. 101832018C176 and 101832020CX087), and from the Jilin Scientific and Technological Development Program, China (No. 20180101287JC).

Conflict of interest On behalf of all authors, the corresponding author states that there is no conflict of interest.

References

1. Z. Shamsollahi, and A. Partovinia, *J. Environ. Manage.* 246, 314 (2019).
2. Y.F. Shen, *J. Agric. Food. Chem.* 65, 995 (2017).
3. Z.F. Wang, A.T. Smith, W.X. Wang, and L.Y. Sun, *Angew. Chem. Int. Edit.* 57, 13722 (2018).
4. I. Kurmanbayeva, A. Mentbayeva, A. Sadykova, A. Adi, Z. Mansurov, and Z. Bakenov, *Eurasian Chem. Technol. J.* 21, 75 (2019).
5. N. Liu, K.F. Huo, M.T. McDowell, J. Zhao, and Y. Cui, *Sci. Rep.* 3, 1919 (2013).
6. W.X. Wang, J.C. Martin, X.T. Fan, A.J. Han, Z.P. Luo, and L.Y. Sun, *ACS Appl. Mater. Interfaces* 4, 977 (2012).
7. H.Y. Chu, Q.Z. Wu, and J.G. Huang, *Colloid Surf. A-Physicochem. Eng. Asp.* 558, 495 (2018).
8. Y.T. Guo, X.D. Chen, W.P. Liu, X.F. Wang, Y. Feng, Y.X. Li, L.J. Ma, B. Di, and Y.M. Tian, *J. Electron. Mater.* 49, 1081 (2020).
9. L.P. Wang, J. Xue, B. Gao, P. Gao, C.X. Mou, and J.Z. Li, *RSC Adv.* 4, 64744 (2014).
10. J.L. Cui, F.P. Cheng, J. Lin, J.C. Yang, K. Jiang, Z. Wen, and J.C. Sun, *Powder Technol.* 311, 1 (2017).
11. G. Lener, A.A. Garcia-Blanco, O. Furlong, M. Nazzarro, K. Sapag, D.E. Barraco, and E.P.M. Leiva, *Electrochim. Acta* 279, 289 (2018).
12. O. Rosales-Calderon, and V. Arantes, *Biotechnol. Biofuels* 12, 240 (2019).
13. H.X. Zhang, X.F. Ding, X. Chen, Y.J. Ma, Z.C. Wang, and X. Zhao, *J. Hazard. Mater.* 291, 65 (2015).
14. T.N. Ang, G.C. Ngoh, and A.S.M. Chua, *Bioresour. Technol.* 135, 116 (2013).
15. F.H. Isikgor, and C.R. Becer, *Polym. Chem.* 6, 4497 (2015).
16. B.C. Saha, *J. Ind. Microbiol. Biotechnol.* 30, 279 (2003).
17. P. Beguin, and J.P. Aubert, *FEMS Microbiol. Rev.* 13, 25 (1994).
18. L. Brinchi, F. Cotana, E. Fortunati, and J.M. Kenny, *Carbohydr. Polym.* 94, 154 (2013).
19. S.K. Singh, and P.L. Dhepe, *Bioresour. Technol.* 221, 310 (2016).
20. E.P. Dagnino, F.E. Felissia, E. Chamorro, and M.C. Area, *Chem. Eng. Res. Des.* 129, 209 (2018).
21. Y. Feng, X.Y. Liu, L. Liu, Z.Q. Zhang, Y.F. Teng, D.Y. Yu, J.Y. Sui, and X.F. Wang, *ChemistrySelect* 3, 10338 (2018).
22. H.X. Zhang, X. Zhao, X.F. Ding, H. Lei, X. Chen, D.M. An, Y.L. Li, and Z.C. Wang, *Bioresour. Technol.* 101, 1263 (2010).
23. Y.X. Li, X.Y. Liu, L. Liu, W.P. Liu, Y. Feng, Y.T. Guo, Y.C. Zhu, J.F. Wang, and X.F. Wang, *J. Electrochem. Soc.* 166, A2425 (2019).
24. D.Y. Kim, Y. Nishiyama, M. Wada, and S. Kuga, *Carbon* 39, 1051 (2001).
25. J. Yu, N. Paterson, J. Blamey, and M. Millan, *Fuel* 191, 140 (2017).
26. Y.M. Feng, L. Tao, Y.H. He, Q. Jin, C.G. Kuai, Y.W. Zheng, M.Q. Li, Q.P. Hou, Z.F. Zheng, F. Lin, and H.B. Huang, *J. Mater. Chem. A* 7, 26954 (2019).
27. L. Tao, Y.B. Huang, Y.W. Zheng, X.Q. Yang, C. Liu, M.W. Di, S. Larpkiattaworn, M.R. Nimlos, and Z.F. Zheng, *J. Taiwan Inst. Chem. Eng.* 95, 217 (2019).
28. D.Z. Shen, C.F. Huang, L.H. Gan, J. Liu, Z.L. Gong, and M.N. Long, *ACS Appl. Mater. Interfaces* 10, 7946 (2018).
29. D.L. Jia, K. Wang, and J.G. Huang, *Chem. Eng. J.* 317, 673 (2017).
30. W.J. Wu, J. Shi, Y.H. Liang, F. Liu, Y. Peng, and H.B. Yang, *Phys. Chem. Chem. Phys.* 17, 13451 (2015).
31. H.H. Li, L.L. Zhang, C.Y. Fan, K. Wang, X.L. Wu, H.Z. Sun, and J.P. Zhang, *Phys. Chem. Chem. Phys.* 17, 22893 (2015).
32. X. Wu, Z.Q. Shi, C.Y. Wang, and J. Jin, *J. Electroanal. Chem.* 746, 62 (2015).
33. Z.M. Xiang, Y.X. Chen, J. Li, X.H. Xia, Y.D. He, and H.B. Liu, *J. Solid State Electrochem.* 21, 2425 (2017).
34. L. Wang, X.X. Zhu, K.K. Tu, D. Liu, H.L. Tang, J.S. Li, X. Li, Z.Z. Xie, and D.Y. Qu, *Electrochim. Acta* 354, 136726 (2020).